# Atomic nature of the Si-B4 paramagnetic center assessed by multifrequency electron spin resonance

K. Keunen and A. Stesmans
*Department of Physics, University of Leuven, Celestijnenlaan 200D, 3001 Leuven, Belgium*
*and Institute for Nanoscale Physics and Chemistry (INPAC), University of Leuven, 3001 Leuven, Belgium*
(Received 16 July 2008; revised manuscript received 5 October 2009; published 17 November 2009)

An electron spin resonance (ESR) study has been carried out in the range 4.2–120 K on the trigonal Si-B4 center in annealed (200–350 °C) neutron-irradiated *p*-type Si. Detailed observations reveal a rich $^{29}$Si hyperfine (hf) structure, indicating interaction of the unpaired electron with up to five shells of equivalent Si sites. Optimized consistent computer-assisted fitting of spectra observed at three ESR frequencies point toward a set of 1-2-2-3-3 equivalent Si sites for the five observed shells in decreasing hf splitting, respectively, with the 1-3-3-3-3 set, conforming with the trigonal symmetry of the defect, giving satisfactory results as well. The strongest interaction of the unpaired electron is with one Si atom. Full angular mapping of all five hf doublets enabled inference of the hybrid coefficients, i.e., localization of the unpaired electron and *s*-*p* ratio over the different Si sites. Stepping from previous theoretical work, two tri-interstitial models are discussed from where, although lack of theoretical results on the molecular wave-function coefficients prevents definite assignment, the tri-interstitial $I_3$-I model is advanced as a plausible candidate. An uncommon drastic temperature dependence is observed in which all resolved $^{29}$Si hf doublet splittings collectively and evenly narrow with increasing temperature toward 1/4 of the low-temperature values along a bounded exponential (Boltzmann factor) decay, with activation energy $E_a \approx 0.0041$ eV. There is an attendant upward shift in $g_{\|}$. An effect due to thermal dilatation as possible origin is excluded. Instead, it is ascribed to even redistribution (delocalization) of the low-temperature unpaired hybrid by 75% over next-neighboring sites, possibly within a four-defect cluster arrangement.

DOI: 10.1103/PhysRevB.80.195207 PACS number(s): 61.72.Hh, 61.80.Hg, 76.30.Mi

## I. INTRODUCTION

During ion implantation, widely used in the fabrication of Si-based devices, intrinsic defects, such as the vacancy (V), self-interstitial (I), and their aggregates, are introduced into the crystalline (c)-silicon substrate. These defects are still being intensively studied because of their role in various dynamic phenomena such as self-diffusion[1] and impurity diffusion,[2] which can influence performance of next-generation electronic devices.

A comprehensive account on the understanding as of year 2000 on Si interstitials, in fact intrinsic defects in Si in general, has been presented in Ref. 3 focusing on results mainly obtained by electron spin resonance (ESR) and to some extend, local vibrational mode spectroscopy in correlation with electrical and optical measurements. As it appears, identification of vacancy-related defects has been far more successful than identification of interstitials. With the aid of ESR and optical measurements one has been able to make convincing identification of various intrinsic vacancy centers (see, e.g., Ref. 4 and references therein) as well as impurity-vacancy pairs (see, e.g., Ref. 5). As to the properties of self-interstitials, in particular isolated Si interstitials, however, knowledge is surprisingly limited. Though with little direct ESR evidence for its existence, a main conclusion attained is that once created, the isolated Si interstitial is highly mobile. More even, with respect to Si device performance, it is considered as a most *dangerous culprit* as it is easily trapped by impurities and other defects, well below ambient temperatures. When trapped by acceptors (B) or C, it forms highly stable, rapidly diffusing entities with low ($\leq$0.8 eV) thermal activation energies. A separate facet concerns the formation of extended defects through aggregation of interstitials ($I_n$), with research results compiled in several works[3,6,7] as obtained by various research methods including photoluminescence (PL), deep level transient spectroscopy, and Fourier transform infrared spectroscopy. Well known here[8,9] are {311} platelets, interstitial aggregates formed as a result of supersaturation of I's. Rather recently though there has been increased interest in interstitial aggregate formation (see, e.g., Ref. 6), largely driven by insightful theoretical progress achieved within the density-functional theory (DFT) approach. Yet, conclusive experimental backup of the different calculated models appears lagging behind.

In 1970, Daly[10] reported the observation by ESR of two paramagnetic centers, labeled Si-B3 and Si-B4, measured in X band at 20 K in irradiated and heat treated *p*-type Si. Both spectra observed correspond to a defect with effective spin $S=1/2$. The Si-B3 spectrum was observed in boron-doped ($2\times10^{17}$ B/cm$^2$) silicon after irradiation with $6.6\times10^{15}$ neutrons/cm$^2$ and annealing at 270 °C for 20 min. The (100) axial symmetry and principal *g*-matrix values were determined. Because of the unusual symmetry (*tetragonal*; $D_{2d}$ point group), the spectrum soon attracted considerable attention.[11,12] In 2003, the tetrainterstitial defect $I_4$, studied in detail in theoretical work[8] based on DFT theory, was, based on experimental results, advanced as the origin of the Si-B3 spectrum by Pierreux and Stesmans[13] as well as Mchedlidze and Suezawa.[7] Since, the assignment of the Si-B3 spectrum was considered rather definite. Yet, more recent in depth and elaborate ESR analysis has revealed that some uncertainties in this assignment remain, which will be dealt with elsewhere.

 

As to Si-B4, the observation by Daly[10] constitutes, to our knowledge, the only ESR report so far made on this defect (apart, likely, from the work in Ref. 14—*vide infra*). The Si-B4 was observed in B-doped ($2\times10^{17}$ B/cm$^3$) irradiated with $5\times10^{17}$ electrons/cm$^2$ and subsequently annealed at 275 °C for 20 min. The spectrum exhibits (111) axial symmetry and $^{29}$Si hyperfine (hf) structure was revealed from interaction with one Si nucleus. The principle hf tensor values are given as $A_{\parallel}=126$ G and $A_{\perp}=78$ G. Daly concluded that the Si-B4 probably concerns a silicon dangling bond (DB) and since, the defect remained unattended. Rather recently, however, Pierreux and Stesmans[14] reported the observation of a similar Zeeman spectrum in heat treated (100) Si after irradiation with high-energy neutrons. The spectrum showed the same symmetry as Daly's Si-B4 and reasonable correspondence in $g$ values. However, the strong hf interaction signals, reported by Daly, were not present in the ESR observations made at 40 K, so the former authors concluded they were dealing with a different defect and labeled it Si-B5. Two weak hf doublets were observed close to the central Zeeman signal. The outer doublet showed a highly isotropic hf splitting with $A_{\parallel}\cong12$ G and $A_{\perp}\cong10$ G. The second hf interaction was only resolved for certain magnetic field angles and has a splitting of $A\cong2.6$ G. Mainly based on the *trigonal symmetry* and the limited hf information, the tri-interstitial was proposed as a possible candidate for the Si-B5 defect. But clearly, in lack of resolution and in-depth analysis of the full hf structure that conclusion could hardly have been more than a first suggestion.

Both the Si-B3 and the Si-B5 have been linked with optical PL centers, namely, the X and W lines (see Ref. 14 and references therein). The latter centers are observed in optical research on irradiated annealed silicon.[15,16] The W center is observed after annealing at temperatures ($T_{an}$) above 200 °C and disappears for $T_{an}\geq350$ °C. At this temperature, the X line arises and remains stable up to $T_{an}$ of about 500 °C. This correlates quite well with the reported annealing behavior of the Si-B3 and Si-B5 defects. Indeed, the Si-B5 center is ESR present after annealing in the range $200\leq T_{an}\leq350$ °C while Si-B3 is detectable in the range $T_{an}=350-450$ °C. Stress studies also showed that the symmetry of the W center is trigonal[17] and the X center is proposed to possess $D_{2d}$ tetragonal symmetry.[18] This again is consistent with the ESR derived properties of the Si-B5 and Si-B3 centers, respectively. In ending this paragraph and before proceeding, concerned about optimized least-confusing defect labeling and in fairness to first disclosure, we here want to anticipate on a result urging some notational reconsideration. As will be discussed further on in this work providing extensive data, the Si-B4, as reported by Daly and the Si-B5, discussed by Pierreux and Stesmans, do most probably concern the same defect. Thus, we will henceforth denote the defect concerned as Si-B4, herewith dropping the Si-B5 label as superfluous.

As mentioned, there has been much theoretical research on interstitial aggregates and several models have been proposed for the tri-interstitial defect.[19–22] Recently, Carvalho *et al.*[23] investigated five different structures for $I_3$, calculating the formation energies, possible band-gap states and the local vibrational states. Three of these models exhibit trigonal symmetry, namely, $I_3$-I, $I_3$-III, and $I_3$-V. However, $I_3$-III is found to be only marginally stable against transformation into $I_3$-II with cubic symmetry. Based on the trigonal symmetry and the model being the only one possessing a band-gap level that could account for PL activity, Carvalho *et al.* advance $I_3$-I as a possible candidate for the W center, as proposed by Coomer *et al.*[20]

The present work extends previous ESR results on the Si-B4 spectrum through an extensive multiobservational frequency ESR study over an extended temperature range with special caution to record undistorted ESR spectra. Emphasis is on providing detailed hf information that could lead to the identification of the ESR Si-B4 spectrum, with up to five $^{29}$Si hf sets being resolved. The possible assignment of Si-B4 to one of the theoretically advanced trigonal $I_3$ models is considered in detail. As an additional pertinent observation, results obtained over the 4.2–120 K temperature range revealed the observed hf splittings and $g$ values to exhibit unusual temperature dependences.

## II. EXPERIMENTAL DETAILS

Slices of $2\times9$ mm$^2$ main area, appropriate for ESR, were cut from (100)Si wafers (thickness ~500 $\mu$m), boron doped to $10^{17}$ cm$^{-3}$, with their 9 mm edge along a $[0\bar{1}1]$ direction. After thorough etching in planar etch $CP_4$ ($HNO_3$:$CH_3COOH$:HF; 7.5:2.5:1 by volume), the slices were irradiated by high-energy neutrons (peak energy ~3 MeV) to a dose of $\sim10^{18}$ cm$^{-2}$. Hereupon, separate samples were vacuum annealed at various temperatures in the range 200–500 °C, to analyze the evolution (ESR spectral properties, symmetry and density) of the various occurring ESR-active defects. As a bonus, this also enables one to select out the most adequate $T_{an}$ window, if existing, for optimum ESR study of an envisioned defect through selective out annealing of interfering defects, i.e., attaining good quality ESR spectra least obscured by other defect spectra. For the current Si-B4 center, the optimal $T_{an}$ appears at ~300 °C; At this temperature, various types of other defects, Si-P3, Si-P6, and Si-H8, have annealed out and the strongly overlapping Si-B3 defect just starts appearing at $T_{an}$ above 300 °C.[14] Accordingly, the samples studied here were vacuum annealed at 300 °C.

Conventional absorption mode ESR observations were carried out in the temperature range $T=4.2-120$ K with the applied magnetic field **B**, at angle $\varphi_B$ with the [100] sample normal **n**, rotating in the $(0\bar{1}1)$ plane, employing X (≈8.9 GHz), K (≈20.5 GHz), or Q-band (≈33.5 GHz) spectrometers driven in the adiabatic slow passage mode, as described elsewhere.[24,25] The amplitude $B_m$ (~0.2 G) of the additionally applied modulation field (typically ~100 kHz) and the incident microwave power $P_\mu$ are appropriately limited in order not to distort the signals. The $g$ values were determined relative to a comounted Si:P marker sample. The signal-to-noise ratio was enhanced by signal averaging (typically around 100–200 scans and in some cases up to 1500 scans).

## III. EXPERIMENTAL RESULTS

Having manufactured c-Si samples quite optimized for the Si-B4 defect, both in terms of signal intensity and reduc-

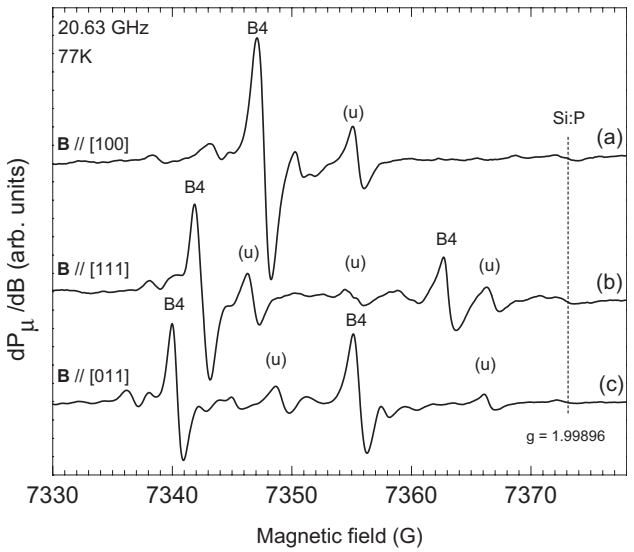


FIG. 1. Representative overview of K-band ESR spectra measured at 77 K for three main orientations of the magnetic field, using $P_\mu$=25 nW and $B_m$=0.25 G. The main Zeeman signals pertaining to Si-B4 are labeled B4 while the signals labeled (u) correspond to as yet unidentified resonances. The signal at $g$=1.99896 stems from a comounted Si:P marker sample.

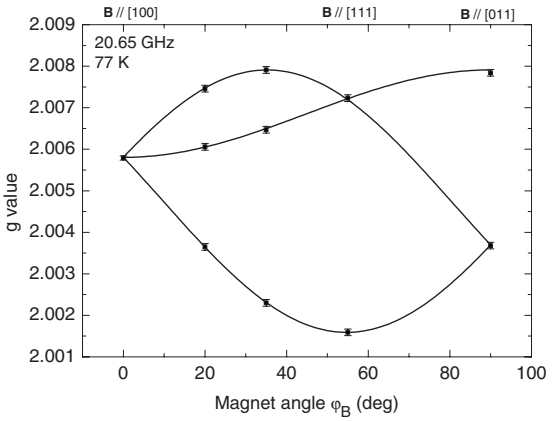


FIG. 2. Angular $g$ pattern of the Si-B4 defect inferred from K-band measurements at 77 K, for **B** rotating in the $(0\bar{1}1)$ plane. The solid lines represent the optimized fitting for trigonal symmetry, using the principal $g$ matrix values $g_\parallel$=2.0016 and $g_\perp$=2.0079. Here, $\varphi_B$ is the angle between the applied magnetic field **B** and the [100] crystal axis.

tion in potentially interfering signals, an extensive ESR study of the Si-B4 spectral properties has been carried out, with a view to provide solid experimental data leading to defect identification. For this end, multifrequency ESR studies have been carried out as a function of temperature, mutual orientation of crystal axes to the magnetic field, and incident microwave power. This has led to noteworthy observations, including revealing of rich hf structure (up to 5 hf doublets) and a remarkable "uncommon" $T$ dependence of this structure, potentially much informative of the defect's structural behavior. Convinced of the potential, much care has been given to ensure recording of undisturbed correct first-derivative ESR signals to enable accurate and reliable relative signal intensity inference, leading to correct assignment of nuclear isotope (shell environment) involvement, the clue to defect identification.

### A. Zeeman signals and hyperfine structure

Figure 1 shows typical K-band ESR spectra, observed at 77 K, for three major orientations of the applied magnetic field, where the resonance field of the codetected isotropic Si:P marker signal at $g(77\ \mathrm{K})=1.99896\pm0.00002$ may serve as common field reference. The principle Zeeman signals are marked as B4, the angular dependence of which will provide the $g$ map and hence, the point symmetry of the defect. Interestingly, on closer perusal, one may perceive additional weak symmetrically positioned structure near the main signals. As this likely concerns hf structure, obviously its study would be a focal point of experimental efforts in unraveling the nature of the defect. Much effort was given to reveal and quantify the occurring hf structure to utmost detail and accuracy. However, unlike the measurement of the principle signals that exercise went far less smooth. Indeed, besides the Si-B4 signals, the spectra also contain some so far unidentified and anisotropic signals, some labeled (u) to aid transparency in presentation. These signals, unfortunately, are present in the same magnetic field region as spanned by the Si-B4 signals, for all orientations of the magnetic field, obstructing inference of hf parameters. However, with the aid of measurements at three different frequencies, we succeeded in distinguishing the Si-B4 hf structure from unrelated signals not belonging to the Si-B4 spectrum. The inferred $g$ pattern at 77 K for **B** rotating in the $(0\bar{1}1)$ plane, shown in Fig. 2, exhibits trigonal symmetry around the [111] axis with principal $g$ matrix values $g_\parallel(\parallel[111])=2.0016\pm0.0001$ and $g_\perp=2.0079\pm0.0001$.

Figure 3 depicts zoomed-in parts of K-band ESR Si-B4 spectra of measurements carried out for five different temperatures with $\mathbf{B}\parallel[100]$ [cf. signal B4 in spectrum (a) of Fig. 1]. Only the low magnetic field part of the central Zeeman line is shown because the high-field slope is obscured by foreign unidentified signals, which distracts analysis. Focusing on the spectra taken at 4.2 and 10 K, four elements of hf structure, labeled (a)–(d) in decreasing order of hf splitting, similarly appearing for the three frequencies, are resolved. Though disturbed by unrelated signals, it was ascertained from the multifrequency ESR studies that this low-field hf structure (a)–(d) is closely symmetrically mirrored at the high-field side with respect to the main Zeeman signal, so we refer to this structure as comprised of four doublets (a)–(d).

The search for detailed hf structure, however, has not been restricted to the near-main signal field range. Figure 4 shows K-band ESR spectra obtained at five different temperatures (again $\mathbf{B}\parallel[100]$) for a larger magnetic field sweep. As can be clearly seen from the 10 and 20 K spectra, one more pair of hf signals is observed, labeled (e), centered at $g_c$ of, and belonging to, the central Zeeman signal, with a splitting about an order of magnitude larger than the previously resolved four hf doublets (a)–(d) close to the central Zeeman line (cf. Fig. 3). Despite intensive search, only one such broad-splitting doublet related with Si-B4 could be traced,

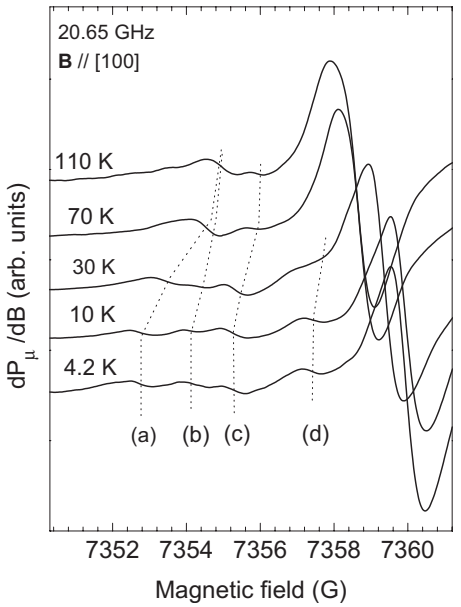


FIG. 3. Detail of the low-field central part of experimental K-band Si-B4 spectra, observed at five different temperatures, with the applied magnetic field **B** along [100] and using $B_m$=0.2 G. Applied $P_\mu$ at 4.2 K is ≈8 pW, increasing to ≈80 nW at 110 K. The dotted lines serve as guide for the eye in exposing the evolution of the four hf structures as a function of temperature.

the spectral properties of which were carefully monitored in order to enable correct comparison of relative signal intensities, i.e., hf signal versus central Zeeman signal. It was ascertained from X-band measurements that other occurring signals are not part of the Si-B4 hf structure since their position relative to the main Zeeman signal of the Si-B4 center depends on the observation frequency and no symmetrically mirrored signal could be traced for any of these signals. Taken together, as is clear from Figs. 3 and 4, we can divide the hf structure into two *groups*, one doublet with large splitting and four weaker hf interactions with splittings remaining close to the central Zeeman line.

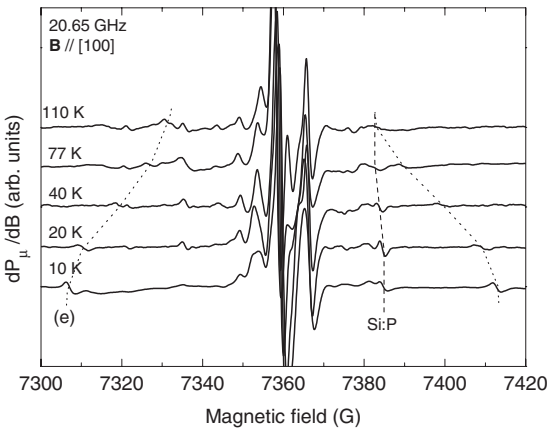


FIG. 4. Observed K-band spectra for five different temperatures with **B**∥[100] and using $B_m$=0.65 G, revealing the occurrence of a hf doublet of large splitting centered at $g_c$ of the central Zeeman signal. The applied $P_\mu$ increases from about 0.1 nW (10 K) to ≈80 nW (110 K). The dotted curves provide an aid to the eye in following the hf doublet of largest splitting as a function of temperature.

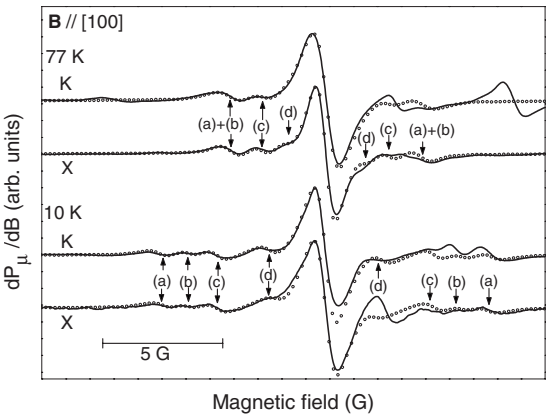


FIG. 5. Computer simulations (open circles) of X- and K-band ESR spectra (solid curves) observed for two temperatures (10 and 77 K) with **B**∥[100] using $B_m$=0.2 G. At 10 K, the applied $P_\mu$ is ≈8.6 $\mu$W and 25 nW for X and K bands, respectively. Simulations correspond to interaction with $^{29}$Si nuclei in shells comprising (a) two, (b) two, (c) three, and (d) three equivalent Si sites. The hf doublets (a)–(d) are indicated, showing that they are reproduced in both frequencies, albeit overlapped by other still unidentified signals. The temperature dependence of the hf structure is also clearly visible.

The Si-B4 spectrum can be described by the simplified spin Hamiltonian composed of the electronic Zeeman interaction and the hf interaction terms,

$$\mathcal{H} = \beta \mathbf{B} \cdot \hat{g} \cdot \mathbf{S} + \sum_j \mathbf{I}_j \cdot \hat{A}_j \cdot \mathbf{S}, \quad (1)$$

with effective electronic spin $S=1/2$. Here $\beta$ represents the Bohr magneton, $\hat{g}$ is the electronic $g$ dyadic, $I$ the nuclear spin, and $\hat{A}_j$ the hf tensor for the interaction of the electronic spin with nuclei of the $j$th group of equivalent lattice sites; for the present case, $j=1-5$. The revealed hf structure is ascribed to interaction with $^{29}$Si nuclei (4.67% abundant, $I=1/2$).

Computer simulations, based on formula (1), have been carried out on spectra taken at the various temperatures for all three ESR frequencies. Special care was taken to convincingly reproduce the various hf spectral features, including *second-order structure* (resulting from multiple site occupation by $^{29}$Si nuclei and intershell interaction). Figure 5 shows examples of such computer simulations (open circles) for X and K-band spectra at two different temperatures (10 and 77 K) for **B**∥[100]. While not all the experimental results could be perfectly fitted with one same set of hf parameters, best overall results were obtained with the configuration in which the defect unpaired electron hybrid has its strongest hf interaction with one $^{29}$Si nucleus [doublet (e)], the next two interactions with a second and third shell each containing two equivalent Si sites [respectively (a) and (b)] and the last two interactions with a fourth and fifth shell each incorporating three equivalent Si sites [respectively (c) and (d)]—referred to as a set of 1-2-2-3-3 equivalent Si sites. It is clear from Fig. 5 that the hf structure is not dependent on observational

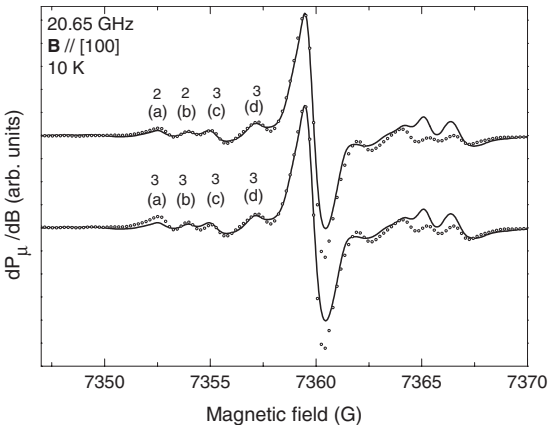


FIG. 6. Comparison of computer simulations (open circles) of a K-band ESR spectrum (solid curves), taken at 10 K with $\mathbf{B}\|[100]$, using a set of 1-2-2-3-3 (top curve) or 1-3-3-3-3 equivalent Si sites, showing the small difference in relative hf doublet intensity with respect to the central Zeeman line.

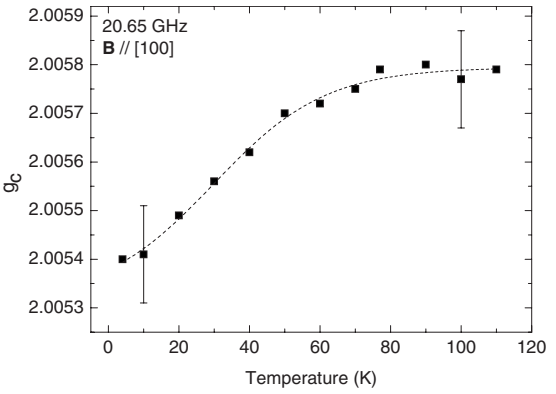


FIG. 7. Temperature dependence of the zero crossing $g$ value $g_c$ of the central Zeeman signal [cf. spectrum (a) in Fig. 1] observed in K-band spectra taken with **B** along [100].

frequency, which is supported by Q-band results as well (not shown).

As alluded in the introduction, the Si-B4 center has been advanced as a (potential) $I_3$-type defect. At this point it may then be pertinent to note that, for a defect with trigonal symmetry, it is rather unlikely to encounter unpaired spin interaction with one Si site, as well as with two shells comprised of two Si sites each. This would seem only possible if all five atoms were positioned on the axis of symmetry of the defect. In this respect, it should be added, in fairness, that conclusive assignment of the number of interacting equivalent Si sites for the inner four doublets [(a)–(d)] from simulation of the experimental spectra may not be as straightforward as hoped for, being complicated by the different hf doublets overlapping with each other, with foreign unidentified signals, and with the intense central Zeeman signal. This, together with the relatively low natural abundance of the $^{29}$Si (4.67%) isotope, makes unambiguous relative intensity determination difficult. So, as it is more likely to find shells of three rather than two equivalent atoms in a trigonal center, simulations were also performed with a set of 1-3-3-3-3 equivalent Si sites for the hf doublets (e)-(a)-(b)-(c)-(d), respectively. Such set would be more plausible for a defect with trigonal symmetry. Additionally, simulations with several other Si shell sets have been attempted, indicating that even sets of 1-2-3-3-3 and 1-3-2-3-3 may deserve attention. While the 1-3-3-3-3 set of equivalent Si sites also gives acceptable fitting results, it appears somewhat inferior to the simulations using the 1-2-2-3-3 set. The (ir)relevance of this may be appreciated from Fig. 6, comparing the results of optimized fitting (open circles) for both sets of Si shells to a high quality K-band spectrum (10 K; $\mathbf{B}\|\mathbf{n}$) encompassing the central [(a), (b), (c), (d)] hf structure, so conclusions may be drawn individually.

Whatever preference, pure fitting results would favor the 1-2-2-3-3 set over the 1-3-3-3-3 one. But with inclusion of uncertainty, the latter cannot be discarded outright, the more since it would comply better with trigonal symmetry of the defect. So, for reasons of consistency and scientific objectivity, we will conduct further analysis based on the 1-2-2-3-3 set but keeping in mind that the main experimental parameters inferred would not be much affected by the 1-3-3-3-3 set approach. In fact, as evidenced by Fig. 6, the difference among sets would, rather than structure, concern the precise relative intensities of the various resolved sets of hf structure involved. Though required for reliable atomic modeling, we note the latter has not been a prime issue in many previous works.[26] As known, relative (hf) signal intensities may be affected by obscuring factors such as changing linewidth and line shape with increasing hf splitting compared to the central Zeeman signal.

### B. ESR spectra temperature dependence

A striking observation is that the hf splittings of the various doublets are strongly dependent on temperature, as clearly demonstrated by the K-band data in Figs. 3 and 4 where the temperature behavior for the various splittings is indicated by dotted curves. This $T$ dependence of the hf splittings is equally observed for all three microwave frequencies used, as may be evident from the X- and K-band results shown in Fig. 5. Also, while the hf splittings change with $T$, there is no noticeable change in defect density (signal intensity). Neither is there any change in relative intensity of the Zeeman and hf signals, as evidenced by spectra simulations (*vide infra*). As also evident from Fig. 3, the $g$ value of the Si-B4 shows a $T$ dependence as well, noticeable by the shift of the central Zeeman line toward lower magnetic field values for higher temperatures. The shift in central zero crossing $g$ value, $g_c$, is shown in Fig. 7, and is found equal for all three ESR frequencies within experimental error. In Fig. 8, the inferred principal $g$ values $g_\parallel$ and $g_\perp$ are given for the temperature range 10–110 K. Noteworthy is that while $g_\parallel$ clearly increases well beyond experimental error, $g_\perp$ seems to be independent on temperature. For both $g_c$ and $g_\parallel$ this shift seems to saturate for temperatures above $\approx$90 K.

The evolution of the splittings of the five hf doublets as a function of $T$ is displayed in detail in Fig. 9, where two observations clearly stand out: first, all five hf splittings show the same tendency in that the splitting decreases with increasing $T$ and second, the decrease in splitting for all col-

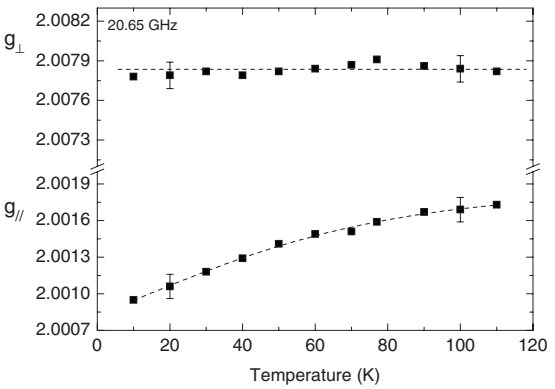


FIG. 8. Temperature dependence of the principal $g$ matrix values of the Si-B4 center as inferred from K-band measurements.

lectively seems to tend to saturation equally at high $T$ ($T > 120$ K). This will be readdressed in more detail below.

### C. Angular dependence

In addition to the behavior of the main Zeeman signals, the angular dependence of the observed hf structure has been studied in detail as well. In Fig. 10 zoomed-in parts of typical X-band spectra, taken at 10 K, are shown together with computer simulations (circles); the signal shown for $\mathbf{B}\|[011]$ corresponds to the low magnetic field branch [see Fig. 1(c) for clarity], this spectral region being the least perturbed by interfering signals. Computer simulations of spectra are compiled in Fig. 11, showing the hf splitting pattern, measured for $\mathbf{B}$ rotating in the $(0\bar{1}1)$ plane, at two frequencies (X and K bands) for two temperatures (10 and 77 K). Here, $\theta$ represents the angle of $\mathbf{B}$ with the $g_{\|}$ direction (assumedly $p$-orbital direction $\langle 111\rangle$) of the defect under study. Open and solid symbols correspond to X- and K-band data, respectively. All doublet splittings, except one, show significant angular dependence. The solid lines represent optimized fittings of the angular dependence of the five hf structures using

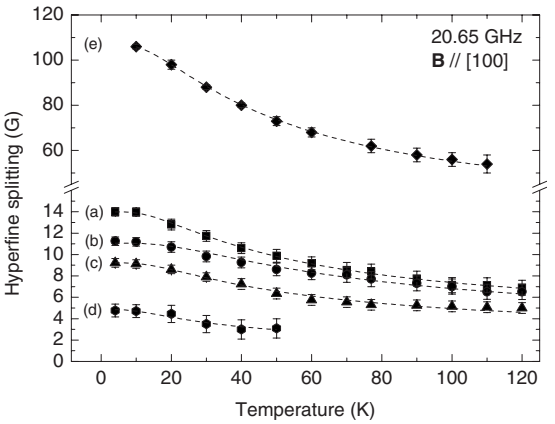


FIG. 9. Temperature dependence of the five $^{29}$Si hf splittings (doublets) as inferred from K-band measurements for $\mathbf{B}\|[100]$. The dashed lines represent least-square fittings of the hf splitting narrowing using Eq. (8).

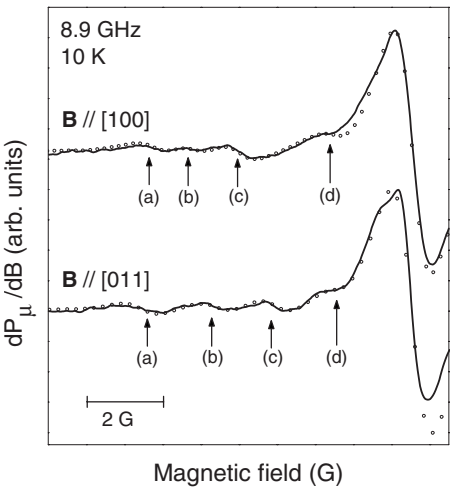


FIG. 10. Part of observed X-band Si-B4 spectra (solid lines), taken at 10 K, for two directions of the magnetic field $\mathbf{B}$. Open symbols correspond to computer simulations based on interaction with four Si shells comprising (a) two, (b) two, (c) three, and (d) three equivalent Si sites. The position of the hf doublets (a)–(d) is indicated for both orientations of the magnetic field.

$$A^2(\theta) = A_{\|}^2 \cos^2(\theta) + A_{\perp}^2 \sin^2(\theta), \tag{2}$$

with the inferred values of $A_{\|}(\|[111])$ and $A_{\perp}$ for both temperatures given in Table I. Almost all experimental spectra are well fitted using five Si shells with 1-2-2-3-3 or 1-3-3-3-3 equivalent sites for the hf doublets (e)-(a)-(b)-(c)-(d), respectively.

## IV. ANALYSIS AND INTERPRETATION

As the unpaired Si-B4 electron is assumed to reside in an unpaired Si orbital, the delocalized paramagnetic defect electron wave function $|\psi(x)\rangle$ may be approximated by a molecular orbital constructed as a linear combination of atomic $sp$-type hybrids[5]

$$\psi_i = \alpha_i |\psi_{s,i}(x)\rangle + \beta_i |\psi_{p,i}(x)\rangle \tag{3}$$

centered on Si atoms at or near the defect, as

$$|\psi(x)\rangle = \sum_i \eta_i (\alpha_i |\psi_{s,i}(x)\rangle + \beta_i |\psi_{p,i}(x)\rangle), \tag{4}$$

where normalization requires $\Sigma_i \eta_i^2 = 1$ while $\alpha_i^2 + \beta_i^2 = 1$. Here, $\eta_i^2$ is the wave-function density at the $i$th group of equivalent sites, and $\alpha_i^2$ and $\beta_i^2$ give the fraction $s$ and $p$ characters, respectively. For axial symmetry, the magnitude of the hf splitting can directly be related to the defect wave function through the relations

$$A_{\|}^i = a_i + 2b_i \quad A_{\perp}^i = a_i - b_i, \tag{5}$$

where $a_i$ and $b_i$, given as

$$a_i = (\mu_0/4\pi)(8\pi/3) g\beta g_{N_i}\beta_N |\psi_{s,i}(0)|^2 \alpha_i^2 \eta_i^2, \tag{6}$$

$$b_i = (\mu_0/4\pi)(2/5) g\beta g_{N_i}\beta_N \langle r_{p,i}^{-3}\rangle \beta_i^2 \eta_i^2, \tag{7}$$

represent the isotropic ($s$ part, Fermi contact interaction) and anisotropic ($p$ part, dipolar interaction) parts of the hf inter-

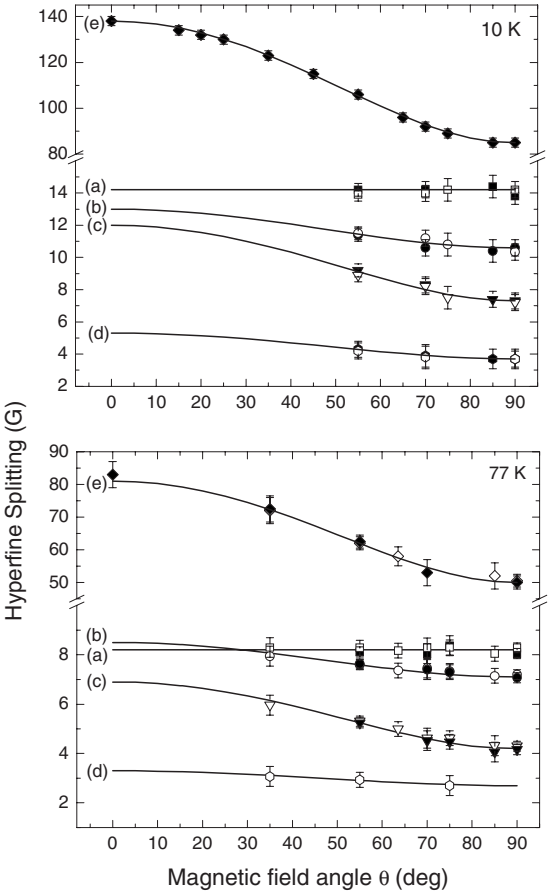


FIG. 11. Angular dependence of observed hf doublets for two temperatures, for **B** rotating in the $(0\bar{1}1)$ plane, where open and solid symbols correspond to X- and K-band results, respectively. The solid curves represent optimized fittings of the angular dependence of the five hf doublets using Eq. (2), from where the principle hf tensor values (cf. Table I) are extracted.

action. Here $g_{N_i}$ is the nuclear $g$ factor of the $i$th group of equivalent sites, $\mu_0$ the vacuum permeability, and $\beta_N$ the nuclear magneton. Such linear combination of atomic orbitals (LCAOs) analysis has been carried out for the current observations, with the results given in Table I for the analysis based on the 1-2-2-3-3 set of equivalent Si sites. As inferred from the first-order hf doublets, the values given for $\eta^2$ correspond to the wave-function density per equivalent Si site. The values used for $|\psi_{s,i}(0)|^2$ and $\langle r_{p,i}^{-3}\rangle$ are those for neutral Si tabulated in Ref. 27, i.e., $|\psi_{s,i}(0)|^2=3.49\times10^{25}$ cm$^{-3}$ and $\langle r_{p,i}^{-3}\rangle=1.82\times10^{25}$ cm$^{-3}$.

Table I again suggests the $T$ dependence of the observed five hf doublets. Both $A_\parallel$ and $A_\perp$ decrease at 77 K to about 60% of their value at 10 K. Another noteworthy observation is that while the localization of the wave function $\eta^2$ decreases with about 40–50 % for all five shells of equivalent Si sites when increasing $T$ from 10 to 77 K, the relative $s$ and $p$ characters of the different shells, $\alpha^2$ and $\beta^2$, stays more or less constant. Only the fifth shell (d) seems to show a small temperature dependence of $\alpha^2$ and $\beta^2$ but parameters for this hf interaction were difficult to resolve at 77 K since, at this $T$, it is situated very close to the main Zeeman signal. A small absolute change in either $A_\parallel$ or $A_\perp$ will translate into a significant change in $\alpha^2$ and $\beta^2$. Thus, as overall picture, we may conclude the $s$-$p$ hybrid ratio corresponding to the various doublets to be largely $T$ independent for all five shells of resolved $^{29}$Si hf interaction.

## V. DISCUSSION

### A. Si-B4 defect model

As stated, a main goal of the current effort is providing a detailed and solid experimental ground to enable tracing the atomic nature of the Si-B4 defect. More specifically we want to examine the possibility, as previously suggested,[14] it to concern basically a Si tri-interstitial. As mentioned in the introduction, according to theory three of the five models advanced for the tri-interstitial in silicon possess trigonal symmetry. The $I_3$-III center, however, is found to relax[28] to $I_3$-II and therefore, will not be discussed here as a possible candidate for the ESR Si-B4 center. The $I_3$-I model, shown in Fig. 12(a) was first proposed by Coomer *et al.*[20] and is com-

TABLE I. Principal hyperfine tensor parameters, $A_\parallel$ and $A_\perp$, for the five shells of equivalent sites and the corresponding molecular wave-function coefficients ($\alpha^2$, $\beta^2$, and $\eta^2$) inferred for the Si-B4 center for two observation temperatures.

| Doublet label | No. of equiv. Si sites | $T_{obs}$ (K) | $A_\parallel$ (G) | $A_\perp$ (G) | $\alpha^2$ | $\beta^2$ | $\eta^2$ (%) |
|---|---|---|---|---|---|---|---|
| (e) | 1 | 10 | $138\pm2$ | $85\pm2$ | 0.13 | 0.87 | 49.6 |
| | | 77 | $81\pm4$ | $50\pm4$ | 0.13 | 0.87 | 29.0 |
| (a) | 2 (3) | 10 | $14.2\pm0.2$ | | 1 | 0 | 0.9 |
| | | 77 | $8.2\pm0.4$ | | 1 | 0 | 0.5 |
| (b) | 2 (3) | 10 | $13.0\pm0.2$ | $10.6\pm0.2$ | 0.26 | 0.74 | 2.7 |
| | | 77 | $8.5\pm0.4$ | $7.1\pm0.2$ | 0.29 | 0.71 | 1.6 |
| (c) | 3 | 10 | $11.8\pm0.4$ | $7.2\pm0.2$ | 0.12 | 0.88 | 4.3 |
| | | 77 | $6.9\pm0.4$ | $4.2\pm0.2$ | 0.12 | 0.88 | 2.5 |
| (d) | 3 | 10 | $5.1\pm0.6$ | $3.7\pm0.2$ | 0.18 | 0.82 | 1.4 |
| | | 77 | $3.3\pm0.6$ | $2.7\pm0.4$ | 0.26 | 0.74 | 0.7 |

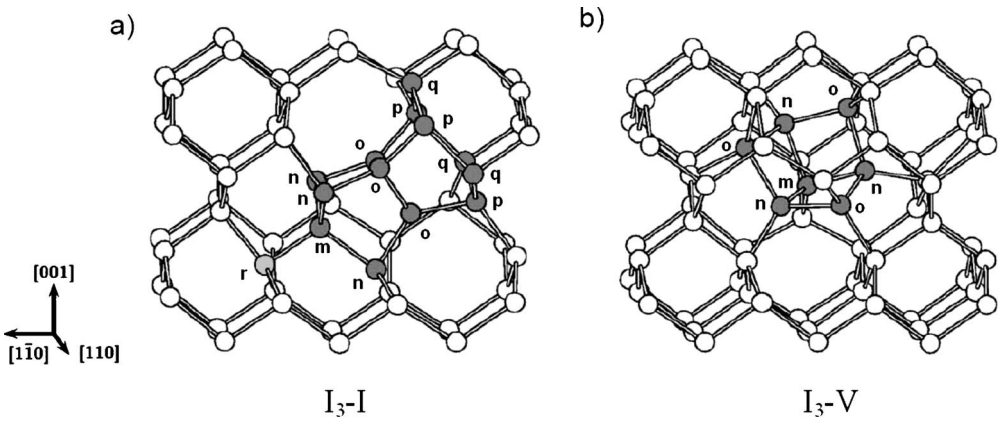


FIG. 12. The two stable trigonal structures of $I_3$, predicted by theory: (a) the $I_3$-I model with $C_{3v}$ symmetry and (b) the $I_3$-V model with $C_3$ symmetry. Figures taken from Carvalho *et al.* (Ref. 23).

posed of three interstitial Si atoms (atoms labeled o) placed at three adjacent bond centered sites, surrounding a tetrahedral interstitial site. All atoms have fourfold coordination. This model possesses $C_{3v}$ symmetry and was proposed as a possible candidate for the optical W center. The defect has been found to be the only tri-interstitial (under study) that produces donor activity and the (0/+) level has been calculated to lie close to the valence-band edge ($\sim E_v+0.19$ eV).[23] In 2004, Richie *et al.*[22] reported on another tri-interstitial with trigonal symmetry. This model, labeled $I_3$-V, is an extended tri-interstitial with $C_3$ symmetry, build up by three four-member rings that form three sides of a distorted cube, as is shown in Fig. 12(b). Again, all atoms in this configuration are fourfold coordinated. Since only $I_3$-I has been calculated to possess a level in the band gap, this structure seems to be the only tri-interstitial that could be a candidate for the Si-B4 center because ESR can only detect defects with an unpaired spin. Yet one "drawback" of this structure may appear the high formation energy as compared to the other tri-interstitial models.[28]

Our experimental results can be optimally reconciled with the interpretation that the Si-B4 defect has its wave function distributed over five shells of equivalent Si sites, the strongest interaction being with one Si site. Focusing on the results obtained at 10 K, about 50% of the wave function is localized on this atom (cf. Table I). The next interaction of the Si-B4 defect is with two shells of two equivalent Si sites each with, respectively, 0.9% and 2.7% localization of the wave function on each atom, followed by interaction with two shells each comprised of three equivalent Si sites. Localization on each of these three atoms at 10 K is 4.3% and 1.4%, respectively.

Then, how well may the provided set of data comply with either of the proposed $I_3$-I and $I_3$-V models? For $I_3$-I, five shells of equivalent atoms are indicated in Fig. 12(a). One shell consists of one atom (atom m) and the other four contain three equivalent atom sites each (atoms n, o, p, and q). Only three shells are specified for $I_3$-V, as depicted in Fig. 12(b). Again, one shell consists of one atom (atom m) while two shells are displayed with both three equivalent Si sites (atoms n and o). Obviously, regardless of the number of shells of equivalent Si sites addressed theoretically, the initially advanced 1-2-2-3-3 shell symmetry would be in conflict with both models: While interaction with a single Si atom as well as with two three-atom shells is present in the experiment [doublets (e), (c), and (d)] and both tri-interstitial models, the experimentally inferred interaction with two shells each comprising a pair of equivalent atoms [doublet (a) and (b)] is inconsistent with trigonal symmetry of both models. But, as outlined, adopting the 1-3-3-3-3 set as an equally valid possibility that obstacle disappears and we may conclude good agreement in terms of symmetry for both models, with preference for the $I_3$-I model.

At least two more aspects may be addressed to attain closer insight: First, as the experimental results reveal the interaction with at least five shells and if accepting that the $I_3$ type of defect would essentially be the correct model for the Si-B4 spectrum, further theoretical work would be needed to explore the number of equivalent Si sites for next possible shells of hf interaction. Second, there are the results on the unpaired electron hybrid parameters (cf. Table I). Unfortunately, to our knowledge, no theoretical analysis of the *s*-*p* ratio of the unpaired electron hybrid and distribution over the different Si sites has been published for any of the tri-interstitial models. That information though could prove decisive for the assignment of $I_3$-I or $I_3$-V to the ESR Si-B4 center, or else rejection.

### B. Temperature-dependent spectral structure

#### *1. Salient features*

As to the unveiled $T$ dependence, two remarkable results come to the fore: (1) while the localization ($\eta^2$) of the unpaired electron over the several shells of equivalent Si sites strongly decreases with increasing $T$, the $s$ and $p$ characters ($\alpha^2$ and $\beta^2$) of these shells do not vary and (2) concerning the $g$ matrix, only $g_{\|}$, not $g_{\perp}$, seems to depend (albeit weakly) on $T$. We interpret this behavior as an indication that the atomic structure of the Si-B4 defect does not change drastically with increasing $T$ but rather that the unpaired electron hybrid is redistributed over the neighboring Si sites. The total amount of wave-function density $\Sigma_i \eta_i^2$ that is accounted for on the first five shells decreases strongly in the range 4.2–120 K, i.e., from $\approx$74% at 10 K to $\approx$43% at 77 K (cf. Table I),

indicating that for higher temperatures the unpaired electron would get more and more distributed over more distant silicon neighbors.

The lack of insight leaves an uncomfortable hiatus, so one might wish to get a physical picture, if only in embryo, of the revealed *T*-dependent phenomena. In an attempt, assuming the proposed tentative interpretation of the Si-B4 to be correct, at least in essence, i.e., involving a multiple self-interstitial defect such as the envisioned $I_3$ defect, one might zoom in on some key features. For one, facing the $I_3$-I model [cf. Figure 12(a)], it may appear this defect to concern a rather strained entity, sensitive to dimensional constraints. Then, one might confer some rearrangements occurring with changing temperature as a result of thermal expansion of the lattice, attendant with redistribution of the unpaired electron hybrid. In this view, one may wonder whether the thermal expansivity ($\alpha$) data of Si bear relevance: Pertinently, pure Si exhibits a *negative* $\alpha$ in the range[29] ~17–120 K, culminating in a maximum volumetric shrinkage of ~0.1‰ relative to its 4 K value, reached in the range 100–120 K, approximately congruent indeed with the temperature range spanned by the currently reported variations in $g_{\|}$ and hf splittings (cf. Figs. 7–9), from whereon $\alpha$ turns positive. Appropriately, this supposition can be firmly tested as at around 180 K, the Si lattice expands back to 4 K dimensions, where in this picture one would then expect the principal *g* matrix values and hf splittings to retake the 4 K values. Extending ESR measurements to the range 120–180 K, however, showed no variation in spectral parameters thus countering the *thermal breathing mode* (implicit) model. Clearly also, according to the data inferred on the hybrid configuration of the unpaired electron, given in Table I, the *T* dependence of the hf structure appears not to stem from a sole change in *s*-*p* hybridization either.

#### *2. Origin T-dependence of hf structure*

Though not as a rule for Si, there have been several previous experimental reports in the literature on the *T* dependence of hf structure, generally focusing on the isotropic hf splitting constant $a_{iso}$ [$=(A_{\|}+2A_{\perp})/3$ for an axially symmetric defect]. Generally, in explaining the *T* dependence of spin-Hamiltonian parameters, two main effects have been considered: (1) thermal expansion (implicit) and (2) lattice-vibration (phonon)-induced variations (explicit). The former one is explaining weak variations in central Zeeman-signal parameters, such as changes in *g* value.[26,30] In the latter case, though not strictly uncorrelated, we may discriminate three variants, as appearing in the literature: (a) motional averaging effect, including the (unpaired) electron hopping between differently oriented, crystallographic equivalent defect sites, which results in substantial modification of ESR spectral and hf structure. Archival examples here are the works of Watkins and Corbett, reporting on the observation of the *T* dependence of ESR properties of the Si-E,[5] Si-G6, and Si-G7 (Ref. 31) centers in electron irradiated Si. This concerns a gross affect on the basic Zeeman signals spectral structure and was ascribed to thermally activated reorientation of the defect from one Jahn-Teller distortion to another. For a defect with an anisotropic *g* tensor, such a reorientation will result in a drastic change in *g* value. This results in a lifetime broadening of the different signal branches (corresponding to the separate branches of the *g* map), related to the possible defect orientations equivalent through crystal symmetry. For higher temperatures, motional narrowing will surge and new sets of lines will arise at the average position of the original branches. Clearly, our experimental results do not show such behavior. Apart from a small variation in *g* value, the intensity and position of the main Zeeman signals do not change in the *T* range 4.2–120 K. Rather, as stated, the current observation deals with the *T* dependence of $^{29}$Si hf structure of the principle Zeeman signals; (b) spin-lattice interaction modification, leading to variations in hf splitting, generally limited to the ≤few % range. It has been reported in many cases, such as F centers in alkali halides[32] and $Mn^{2+}$ in $CaCO_3$.[33] For the case of substitutional $^{55}Mn^{2+}$ in MgO, Orbach *et al.*[34,35] explained the decrease in $a_{iso}$ with *T* as due to phonon modulation of the orbit-lattice interaction. As physical idea, the latter concerns a phonon modulation of the crystalline field established by the ions surrounding the paramagnetic defect. Such temperature decrease in $a_{iso}$, explained along the same lines, was also reported for $Mn^{2+}$ in cubic HgSe (Ref. 30) and the As antisite ($As_{Ga}$) in the GaAs semiconductor,[36] with the weak *T* dependence of *g* ascribed to thermal lattice dilatation; (c) Phonon-induced transitions connecting the ground state and close excited states of a paramagnetic defect. The resonant electrons occupy the ground state and excited states according to the Boltzmann factor, and when the transition rate is sufficiently fast, the hf splitting tends to an average value. It may result in substantial changes in hf splitting ($\Delta a_{iso}/a_{iso} \geq 10\%$ range), as, e.g., in the case of donor states in Si.[37,38] For low-moderately P-doped Si, Dugdale *et al.*[37] reported a decrease in $^{31}$P($I=1/2$)$a_{iso}$ from 41 G at 20 K to 32 G at 40 K, which was explained by motional averaging due to phonon-induced transitions between the onefold ground state and the first threefold state of the P donor. Their theory thus deals with defects involving an impurity atom and as devised, would best apply to shallow centers, such as P donors, in semiconductors. But in essence, it is only required that the defect wave function is amenable to the effective-mass approximation, wherein the ground and excited states defect wave functions are written in terms of multivalley conduction-band states.[39]

Regarding the current Si-B4 spectrum, within the $I_3$ model, the correlated substantial strain field would likely result in a deep center, where the strongly localized defect potential violates the assumption within the effective-mass approximation of a defect potential slowly varying in space. In support, the (0/+) donor level has been calculated[23] at $\sim E_v+0.19$ eV, so it is not clear that the effective-mass approximation would be valid. But apart from this objection, we tend to reject the motional averaging model of Ref. 37 as possibly accounting for the Si-B4 properties because it would involve population of excited levels with reduced *s* character but increased *p* character, thus changing the *s*-*p* hybridization, contrary to the experiment (cf. Table I).

In another case, the *T* dependence of the $^{29}$Si hf splittings of the $E_4'$ center in $\alpha$ quartz was explained by Boltzmann repopulation of the Si vibrational levels in the asymmetric

double-minimum potential of the H bond system Si(2)-H-Si(1).[40] Though well distinct from the former model, yet within the spirit of thermal excitation between the ground state and a nearby excited state, a next classic example concerns the $T$ dependence ($g$ factor, $A$ and $\eta$) of the Si-P1 defect, modeled as a five-vacancy cluster:[26] Here, based on simple one-electron LCAO treatment, the $T$ dependence of the crucial hybrid distribution of the localized unpaired electron is pictured as a result of thermal excitation between a simple DB ground state (low $T$ state; $\leq 120$ K) and, as $T$ increases, between a next excited bond-sharing state of higher energy of the defect—spilling over of the unpaired electron wave function mainly localized at one DB on Si atom $A$ to a next one at site $B$ in the defect structure; now, as a result, two DBs participate in the spin resonance.

Stepping from the $I_3$ picture as basic model of the Si-B4 defect, we suggest, within the spirit of the latter class, that the observed $T$ dependence of main ESR properties may be explained within the concept of thermally induced transitions among unpaired electron states, yet in a view widened compared to the intradefect transition scenario outlined for the Si-P1 defect. We consider three basic ingredients of the Si-B4 spectrum: (a) a first main one stems from Fig. 9, exposing all five observed $^{29}$Si hf splittings (for $\mathbf{B}\|[100]$) to show a similar relative narrowing with increasing $T$. Deeper analysis reveals the remarkable finding that all decays, starting at $T \approx 10$ K, can be consistently described by the relation (dashed curves in Fig. 9)

$$A^i(T;\mathbf{B}\|[110]) = A^{i,\max}\left(1 - \frac{3}{4}e^{-E_a/kT}\right), \tag{8}$$

with $A^{i,\max}$ the initial value of the hf splitting at $T \leq 10$ K and $E_a = 0.0041 \pm 0.0004$ eV, indicating exponential hf splitting narrowing governed by the Boltzmann factor. The uniform relatively equal narrowing of the hf splittings is directly evident from the normalized plot of $\ln(1 - A^i/A^{i,\max})$ versus $1/T$ shown in Fig. 13. The data share around a straight line, the fitting of which [Eq. (8)] gives $E_a = 0.0041 \pm 0.0004$ eV. Then referring, within the LCAO analysis, to the one-to-one relationship between hf splitting and hybrid localization density $\eta^2$, it would indicate that the resonant-electron wave function gradually gets more delocalized with increasing $T$, i.e., partly and relatively equal leaking away from the atomic Si sites responsible for the different hf structures. Asymptotically only 1/4 remains in the high-$T$ limit, 3/4 has spread out. (b) As the LCAO interpretation tells us (cf. Table I), this occurs without noticeably changing the $\alpha^2/\beta^2$ hybridization ratios. And, as expected, neither is there any change, within experimental accuracy, in relative intensities of the various hf doublets and the central Zeeman signal, as inferred from the various signal simulations as a function of $T$. (c) Apart from the $T$-dependence aspect, the Si-B4 defect (10 K) shows remarkably close properties to those of a prototypical Si DB in Si, such as the well-known interfacial $P_b$ center in thermal (111) $Si/SiO_2$ (see below and Table II).[41–43]

On this basis, and within the $I_3$ model, we would picture Si-B4 as a positively charged defect when in the ESR-active state, with an unpaired electron mainly localized at site m, *viz.*, in the strained r-m bond (cf. Fig. 12(a)). The likely

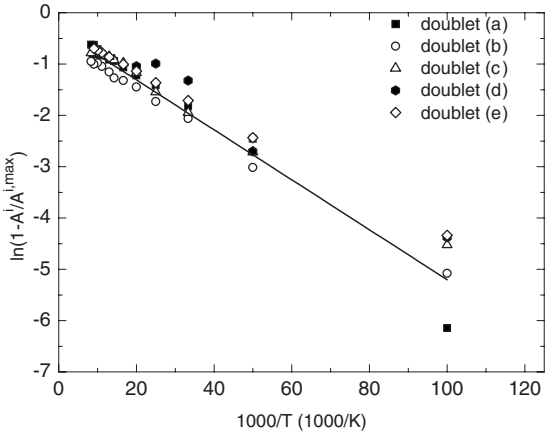


FIG. 13. Normalized plot of the temperature dependence of hf splitting for the five observed $^{29}$Si hf doublets, as obtained from K-band measurements for $\mathbf{B}\|[100]$. The solid line represents an optimized fitting using Eq. (8), showing the uniform bounded exponential narrowing of the various hf splittings with activation energy $E_a \approx 0.0041 \pm 0.0004$ eV.

strained nature of the r-m bond may promote the loss of an electron and with the defect being observed by ESR in $p$-type Si, the second electron may have dropped into an acceptor (B), in agreement with theoretical evaluation of its basic electron level, i.e., at $\approx 0.19$ eV above the VB.[20,23] In this view, we may picture Si-B4 as a basic Si DB axial defect, stabilized by the trigonal symmetry preserving lattice distortion represented by the $I_3$ defect structure.

Based on these considerations, we advance as synoptic picture for the $T$ dependence of the $^{29}$Si hf splittings one in which, as key element, the resonant-electron hybrid, with major density at atom m [r-m bond; Fig. 12(a)] gradually delocalizes with increasing $T$ under thermal impetus. As noticed from 10 K onward, this occurs exponentially, characterized by a small activation energy $E_a \approx 0.0041$ eV. It proceeds to such an extend that 3/4 of the low $T$ ($\leq 10$ K) wave-function density at the central part of the defect [Si sites m, n, o, p, q; Fig. 12(a)] has spilled over, relatively equal from all sites, to other/more remote neighboring Si sites at high $T$. The evenly ebbing away of the wave-function density leaves the $s$-$p$ hybridization ratio of the remaining part intact. In short, the initial low-$T$ resonant-electron hybrid at the Si-B4 ($I_3$) defect is at high $T$ replaced by an identical one, of only 1/4 of the initial density.

In a final step, one may then speculate about how such wave-function spreading may effectively come about. Obviously, one may envision various scenarios. In an extreme academic made-to-measure model, one may hypothesize that the unpaired electron wave function redistribution would occur through thermally driven delocalization over three more defects, otherwise identical except for not being in the ESR-active state initially –the latter adding perhaps even more to the hypothetical aspect. It would thus suppose that Si-B4 centers occur in clusters of four electronically linked defects, i.e., accessible for the resonant electron. As a positive ingredient, it would naturally explain the wave function leakage to saturate at a 3/4 reduction at high temperatures, with unaltered hf structure. In another less exotic view, one may sim-

TABLE II. Comparison of salient ESR parameters of the Si-B4 center in *n*-irradiated B-doped Si and the $P_b$ center at the interface of standard thermal (111)$Si/SiO_2$.

| Defect | Symmetry | $g_{\parallel}$ ($\pm 0.0001$) | $g_{\perp}$ | $A_{\parallel}$ [b] (G) | $A_{\perp}$ [b] (G) | $\alpha^2$ | $\beta^2$ | $\eta^2$ (%) | Equiv. Si sites |
|---|---|---|---|---|---|---|---|---|---|
| Si-B4 (10 K)[a] | Trigonal ($C_{3v}$) | 2.0010 | $2.0079 \pm 0.0001$ | $138 \pm 2$ | $85 \pm 2$ | 0.13 | 0.87 | 49.6 | 1 |
| $P_b$ [c] | Trigonal ($C_{3v}$) | 2.0014[d] | 2.0086[d] $\pm 0.0003$<br>2.0088[h] $\pm 0.0003$ | $156 \pm 5$ [e,f] | $91 \pm 9$ [e] | 0.11[e,g] | 0.89[e,g] | 62[e,g] | 1 |

[a]Current work.
[b]Doublet (e) of largest hf splitting (cf. Fig. 4).
[c]In standard thermal (111)$Si/SiO_2$ grown at $T_{ox} \geq 800$ °C.
[d]See, e.g., Ref. 43.
[e]Reference 41.
[f]Reference 42.
[g]Reference 44.
[h]Reference 45.

ply put that the resonant-electron wave function just increasingly delocalizes over more remote Si sites with increasing $T$. It may inherently be linked with the extended nature of the defect. But obviously, it then needs to be understood why the maximum delocalization would just stop at a 3/4 reduction and why the spilling over occurs with an activation energy of $E_a \approx 0.0041$ eV. In lack of information, this is as far as one can go. Further insight may come from taking a next step in ESR spectrometry, such as *in situ* application of strain or turning to electron-nuclear double resonance experiments. Obviously, further progress will definitely require intensified theoretical study as well.

#### *3. Si DB-type center*

With the Si-B4 ESR spectrum analyzed in more detail, it is noteworthy how the main ESR parameters resemble those of a prototype Si DB defect, namely, the intensively studied $P_b$ center at the thermal (111)$Si/SiO_2$ interface, identified as $Si \equiv Si^{\bullet}$, that is, an unpaired Si DB at a trivalent interfacial Si atom backbonded to three Si's in the substrate. This resemblance is exposed by Table II, listing salient ESR quantities of both centers, where the comparising Si-B4 data are taken at 10 K, i.e., before thermally induced delocalization of the unpaired hybrid and restricted to the $^{29}Si$ hf doublet of largest splitting [doublet (e) in Fig. 4]. The resemblance of the parameters is remarkable, including the hybridization and localization of the unpaired electron hybrid. It appears that of all defects revealed by ESR in Si to date, Si-B4 comes closest in ESR properties to those of the Si DB.[46] It may provoke the critical remark Si-B4 just to concern a *bulk version* of the interfacial $P_b$ center. In the same breath, though, such suggestion about the identical nature of both centers is countered by comparison of other ESR properties, such as the revealed $T$ dependence of other parameters ($g$, hf splittings) of Si-B4, not reported for $P_b$. Neither does the center exhibit[41,42] such additional $^{29}Si$ hf structure as Si-B4 [doublets (b)–(d) in Fig. 5], which has been extensively verified again for this work on an optimized thermal (111)$Si/SiO_2$ sample. Though perhaps not entirely relevant, noticing the outlined resemblance may support theoretical insight on the defect model.

Finally, as a side note it might be useful to mention that, in contrast with Pierreux and Stesmans,[14] we were able to resolve a strong hf interaction of the current center with one Si atom, as was observed by Daly[10] in his report on the Si-B4 signal. Based on the absence of this hf interaction, Pierreux and Stesmans concluded one was dealing with another defect and labeled it Si-B5. They, however, performed measurements at 40 K while the observations by Daly where made at 20 K. With the temperature dependence unveiled in this work it is clear why the same hf interaction could not be resolved by both groups. The principal hf matrix values reported by Daly at 20 K were $A_{\parallel}=126$ G and $A_{\perp}=78$ G. The corresponding molecular wave-function coefficients are $\alpha^2=0.13$, $\beta^2=0.87$, and $\eta^2=45\%$, in perfect agreement with our current results for hf doublet (e). This indicates that the Si-B4 and the Si-B5 spectra most probably concern the same defect.

## VI. SUMMARY AND CONCLUSIONS

The Si-B4 paramagnetic spectrum, observed in irradiated *p*-type Si after annealing in the temperature range 200–350 °C, has been extensively analyzed by ESR in an attempt to determine the atomic structure of the originating defect. The center exhibits trigonal symmetry and a rich hf satellite structure is revealed, ascribed to $^{29}Si$ hf interaction. Using multifrequency observations we were able to resolve up to five hf doublets interpreted as corresponding to five shells each comprising a certain set of equivalent Si sites. Best overall computer-assisted spectral fitting results were obtained using a set of 1-2-2-3-3 equivalent Si sites for the five resolved hf doublets in decreasing hf splitting, respectively, the strongest interaction being with one Si atom. Yet, if focusing mainly on the spectral structure, the set of 1-3-3-3-3 leads to equally satisfactory results, consistent with the trigonal symmetry of the Si-B4 center.

The detailed hf structure, indicating the interaction of the unpaired electron with up to five shells of equivalent Si sites, would be in line with a model involving multiple interstitials, such as the tri-interstitial models. So, in this perspective and together with the trigonal symmetry both the $I_3$-I and $I_3$-V could be good candidates for the Si-B4 center. While the experimental data does not fit perfectly with the theoretical models, the agreement may be considered satisfactory, especially on grounds of the inferred set of 1-3-3-3-3 equivalent Si sites for $^{29}Si$ hf interaction.

From the two models, $I_3$-I is slightly preferable for the Si-B4 since it was calculated to possess a level in the band

gap. Some theoretical groups, however, already claimed this structure to have too high formation energy and thus assumed this structure not to be able to form. Unfortunately, no decisive evidence could be provided to assign the Si-B4 paramagnetic center to one of the two tri-interstitial models. The possible proof, or perhaps the rejection, might come from further theoretical calculations of the molecular wave-function coefficients of the tri-interstitials, i.e., the wave-function density distribution and the *s-p* hybrid ratio.

An uncommon distinct temperature dependence of the hf parameters has been revealed, which, to trace its origin has prompted extensive search of the literature on point defects for precedents. There are the two main observations: First, while the *s-p* hybrid ratio of all five observed hf interactions remains unchanged, all resolved $^{29}$Si hf doublet splittings collectively exhibit a drastic, relatively equal, narrowing with increasing $T$ from $\approx 10$ K onward to 1/4 of the respective low-$T$ values, asymptotically reached at high temperatures ($T > 120$ K). It is described by bounded exponential decay governed by the Boltzmann factor, with an extracted activation energy $E_a \approx 0.0041$ eV. Second, though relatively much weaker, $g_{\parallel}$ monotonously increases with temperature in the range 4.2–120 K while $g_{\perp}$ appears unaffected. Measurements in the range 120–180 K excluded this $T$-dependent behavior to originate from a thermal dilatation effect.

Based on archival knowledge, and guided by LCAO analysis, the $T$ dependence of the $^{29}$Si hf structure is seen to effectuate within a lattice-vibration model in which, as key factor, the resonant-electron hybrid gradually and evenly delocalizes with increasing $T$ (from $\approx 10$ K onward) from the major atom sites comprising the defect to such extend that 3/4 of the initial low-$T$ hybrid occupation has spilled over to (more remote) neighboring sites for $T > 120$ K. Suggestively, it may occur within a four-defect cluster arrangement. Obviously, correct understanding of this revealed unique behavior for a point defect in bulk c-Si is of fundamental interest. Potentially it may be related to the formation of extended aggregates of I's, such as the well-known {311} platelets.

Through comparison of the symmetry, the principal $g$ matrix values and the available hf structure information, it is inferred that the previously reported Si-B4 defect and the Si-B5 spectra most probably concern one and the same defect, herewith making the latter label superfluous.


[1] P. E. Blöchl, E. Smargiassi, R. Car, D. B. Laks, W. Andreoni, and S. T. Pantelides, Phys. Rev. Lett. **70**, 2435 (1993).
[2] A. E. Michel, Appl. Phys. Lett. **51**, 487 (1987); D. J. Eaglesham, P. A. Stolk, H. J. Gossmann, and J. M. Poate, *ibid.* **65**, 2305 (1994).
[3] G. D. Watkins, Mater. Sci. Semicond. Process. **3**, 227 (2000).
[4] B. Hourahine, R. Jones, A. N. Safonov, S. Öberg, P. R. Briddon, and S. K. Estreicher, Phys. Rev. B **61**, 12594 (2000).
[5] G. D. Watkins and J. W. Corbett, Phys. Rev. **134**, A1359 (1964).
[6] B. J. Coomer, J. P. Goss, R. Jones, S. Öberg, and P. R. Briddon, J. Phys.: Condens. Matter **13**, L1 (2001).
[7] T. Mchedlidze and M. Suezawa, J. Phys.: Condens. Matter **15**, 3683 (2003); T. Mchedlidze and M. Suesawa, Phys. Rev. B **70**, 205203 (2004).
[8] P. A. Packan and J. D. Plummer, Appl. Phys. Lett. **56**, 1787 (1990).
[9] A. Agarwal, T. E. Haynes, D. A. Eaglesham, H. J. Gossmann, D. C. Jacobson, J. M. Poate, and Y. E. Erokhin, Appl. Phys. Lett. **70**, 3332 (1997).
[10] D. F. Daly, J. Appl. Phys. **42**, 864 (1971).
[11] K. L. Brower, Phys. Rev. B **14**, 872 (1976).
[12] Y. V. Gorelkinskii, N. N. Nevinnyi, and V. A. Botvin, Radiat. Eff. **49**, 161 (1980).
[13] D. Pierreux and A. Stesmans, Phys. Rev. B **68**, 193208 (2003).
[14] D. Pierreux and A. Stesmans, Phys. Rev. B **71**, 115204 (2005).
[15] E. Terashima, T. Ikarashi, M. Watanabe, and T. Kitano, Mater. Sci. Forum **258-263**, 587 (1997).
[16] O. O. Awadelkarim, A. Henry, B. Monemar, J. L. Lindstrom, Y. Zhang, and J. W. Corbett, Phys. Rev. B **42**, 5635 (1990).
[17] G. Davies, E. C. Lightowlers, and Z. E. Ciechanowska, J. Phys. C **20**, 191 (1987).
[18] Z. Ciechanowska, G. Davies, and E. C. Lightowlers, Solid State Commun. **49**, 427 (1984).
[19] M. Gharaibeh, S. K. Estreicher, and P. A. Fedders, Physica B **273-274**, 532 (1999).
[20] B. J. Coomer, J. P. Goss, R. Jones, S. Öberg, and P. R. Briddon, Physica B **273-274**, 505 (1999).
[21] L. Colombo, Physica B **273-274**, 458 (1999).
[22] D. A. Richie, J. Kim, S. A. Barr, K. R. A. Hazzard, R. Hennig, and J. W. Wilkins, Phys. Rev. Lett. **92**, 045501 (2004).
[23] A. Carvalho, R. Jones, J. Coutinho, and P. R. Briddon, Phys. Rev. B **72**, 155208 (2005).
[24] G. Van Gorp and A. Stesmans, Phys. Rev. B **45**, 4344 (1992).
[25] A. Stesmans, B. Nouwen, and K. Iakoubovskii, J. Phys.: Condens. Matter **12**, 7807 (2000).
[26] Y. H. Lee and J. W. Corbett, Phys. Rev. B **8**, 2810 (1973).
[27] J. R. Morton and K. F. Preston, J. Magn. Reson. (1969-1992) **30**, 577 (1978).
[28] G. M. Lopez and V. Fiorentini, Phys. Rev. B **69**, 155206 (2004).
[29] C. A. Swenson, J. Phys. Chem. Ref. Data **12**, 179 (1983).
[30] T. Gregorkiewicz and S. W. Biernacki, J. Phys. C **13**, 1285 (1980).
[31] G. D. Watkins and J. W. Corbett, Phys. Rev. **138**, A543 (1965).
[32] V. Ya. Kravchenko and V. L. Vinetskii, Opt. Spectrosc.-USSR **18**, 37 (1965).
[33] R. A. Serway, Phys. Rev. B **3**, 608 (1971).
[34] R. Orbach and P. Pincus, Phys. Rev. **143**, 168 (1966).
[35] E. Simanek and R. Orbach, Phys. Rev. **145**, 191 (1966).
[36] A. Mauger, H. J. von Bardeleben, J. C. Bourgoin, and M. Lannoo, Phys. Rev. B **36**, 5982 (1987).
[37] D. E. Dugdale, S. D. Lacey, and G. Lancaster, J. Phys. C **4**, 654 (1971).
[38] G. D. Watkins and F. S. Ham, Phys. Rev. B **1**, 4071 (1970).
[39] P. Yu and M. Cardona, *Fundamentals of Semiconductors* (Springer, Berlin, 2001), p. 161.
[40] J. Isoya, J. A. Weil, and L. E. Halliburton, J. Chem. Phys. **74**, 5436 (1981).
[41] K. L. Brower, Appl. Phys. Lett. **43**, 1111 (1983).

[42] A. Stesmans, Phys. Rev. B **48**, 2418 (1993).
[43] E. H. Poindexter and P. J. Caplan, Prog. Surf. Sci. **14**, 201 (1983).
[44] A. Stesmans, B. Nouwen, and V. V. Afanas'ev, Phys. Rev. B **58**, 15801 (1998).
[45] A. Stesmans, Semicond. Sci. Technol. **4**, 1000 (1989).
[46] C. A. J. Ammerlaan, in *Semiconductors*, edited by O. Madelung, U. Rössler, and M. Schultz (Springer, Berlin, 2002), Vol. 41, p. 236.